Heliyon 10 (2024) e38698

Contents lists available at ScienceDirect

Heliyon

journal homepage: www.cell.com/heliyon

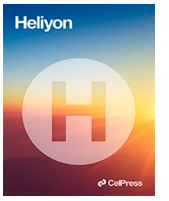

Research article

hUC-MSCs mitigate atherosclerosis induced by a high-fat diet in ApoE$^{-/-}$ mice by regulating the intestinal microbiota

Lin Yang [a,1], Bing Xia [a,1], Tianbao Qian [c,1], Jie Wang [a], Yuanhe Wang [a], Jialin Dai [a], Cuiyun Le [a], Xiaorong Yang [a], Jun Wu [a], Wenxin Wu [a], Jianwei Xu [d,**], Youbin Liu [e,***], Jiawen Wang [a,b,*]

[a] School of Forensic Medicine, Guizhou Medical University, Guiyang, 550000, Guizhou, China
[b] School of Basic Medicine/Institute of Forensic Medicine, Gannan Medical University, Ganzhou, 341000, Jiangxi, China
[c] School of Biology and Engineering, Guizhou Medical University, Guiyang, 550000, Guizhou, China
[d] Center for Tissue Engineering and Stem Cell Research, Guizhou Medical University, Guiyang, 550004, Guizhou, China
[e] Cardiovascular Department of Ganzhou People's Hospital, Ganzhou, 341099, Jiangxi, China

ARTICLE INFO

Keywords:
hUC-MSCs
Intestinal flora
Atherosclerosis
Young's modulus
Plaque stability

ABSTRACT

Background: The mechanism underlying human umbilical cord mesenchymal stem cells (hUC-MSCs) regulating the stability of atherosclerotic plaque was explored by establishing mice models of atherosclerosis induced by a high-fat diet and hUC-MSCs intervention.
Methods: The ApoE$^{-/-}$ mice atherosclerosis model was constructed using a high-fat diet, and mice were divided into a normal diet group (ND), high-fat diet group (HFD), hUC-MSCs treatment group (HFDM), while the blank control (BC) consisted of C57BL/6J mice. After successful establishment of the model, the feces, hearts, and aorta of mice were collected. Morphological features were detected using HE, oil red O, and Masson staining. Afterward, 16s rRNA gene sequences was used to detect the species and abundance of the intestinal flora in mice, and an atomic force microscope (AFM) was used to detect the Young's modulus of the fibrous cap of atherosclerotic plaques. Lastly, the expression level of the inflammatory factors NLRP3, IL-1β, and IL-18 were detected via immunohistochemistry and immunofluorescence assays.
Results: In terms of morphological characteristics, the expression level of NLRP3, Young's modulus of the fibrous cap, and plaque stability were significantly reduced in HFD, whereas the ratio of Firmicutes to Bacteroidetes (F/B) was significantly increased. Interestingly, hUC-MSCs treatment reversed the above indices, thus enhancing plaque stability.
Conclusion: HFD led to dysregulation of intestinal flora homeostasis and induced aberrant expression levels of NLRP3, resulting in a decrease in the Young's modulus of plaques. However, hUC-MSCs treatment improved the biomechanical properties of plaque by modulating the intestinal flora and NLRP3, thereby elevating plaque stability and minimizing the risk of plaque rupture.

* Corresponding author. School of Forensic Medicine, Guizhou Medical University, Guiyang, 550000, Guizhou, China.
** Corresponding author.
*** Corresponding author.
E-mail addresses: 363912577@qq.com (J. Xu), liuyoubin2021@163.com (Y. Liu), wjwwfs@126.com (J. Wang).
[1] These authors contributed equally to this work and should be considered as co-first authors.

https://doi.org/10.1016/j.heliyon.2024.e38698
Received 29 January 2024; Received in revised form 26 September 2024; Accepted 27 September 2024
Available online 28 September 2024

1. Introduction

Cardiovascular disease (CVD) is a pervasive ailment that afflicts individuals worldwide and is a leading cause of sudden death [1]. Presently, CVD exerts a profound influence on individuals' lives and physical well-being. Among the various forms of CVD, coronary atherosclerotic heart disease (CHD) reigns supreme as the most prevalent and foremost cause of sudden death.

Atherosclerosis (AS) serves as the pathological foundation of CHD. Throughout its progression, pathological alterations, such as lipid accumulation, inflammatory cell infiltration, and vascular smooth muscle cell (VSMC) proliferation, occur [2]. The sudden rupture of non-severely stenotic atherosclerotic plaques due to destabilization is the root cause of acute coronary syndrome [3]. Currently, unstable plaques are defined by a higher infiltration of inflammatory cells, such as macrophages and lymphocytes, a thin fibrous cap, and a limited number or absence of VSMCs [4]. Previous research has demonstrated that the size of the lipid core and the thickness of the fibrous cap are the primary factors influencing plaque stability. Nevertheless, the mechanical environment in which atherosclerosis develops is also a crucial influencing factor. As is well documented, the biomechanical properties of atherosclerotic plaques are closely linked to stability [5]. A study has indicated that precise quantification of morphological and biomechanical properties is a key parameter for defining the stability of diseased arterial plaques [6]. The unpredictable rupture of unstable plaques predisposes individuals to adverse cardiovascular events, such as acute coronary syndrome or even sudden cardiac death [7]. Atomic force microscopy (AFM) has been widely used in various fields for its excellent nanoscale measurement performance [8,9] and has also been applied to detect the biomechanical properties of different sections of atherosclerotic plaques [10,11]. Therefore, AFM was utilized to determine the biomechanical properties of the fibrous cap of plaques, and plaque stability was assessed in conjunction with its morphological features.

It is universally recognized that the pathological state of the host is typically accompanied by dynamic changes in the microbial status of the intestinal tract. The normal structural composition of the intestinal flora not only provides nourishment to the host but also governs metabolism, promotes the development of the intestinal epithelium, and induces innate immunity. Disruption of the normal structure and composition of the intestinal flora can impair the health of the host and lead to the development of various diseases, including atherosclerosis and hypertension [12]. In addition to intestinal flora imbalance, infections are hypothesized to exacerbate atherosclerosis [13]. In short, different flora plays different roles in the intestine. For instance, Bacteroides vulgatus and Bacteroides dorei have been shown to inhibit the synthesis of lipopolysaccharides by intestinal microorganisms, thereby minimizing the risk of atherosclerosis [14]. In addition, bacteria such as Roseburia, Klebsiella, Clostridium IV, and Ruminococcaceae showed abundance changes in different stages of cardiovascular disease [15]. Overall, a multitude of bacteria have been shown to participate in the development of atherosclerosis, and maintaining the dynamic balance of the intestinal flora is key for the treatment of atherosclerosis. Therefore, modulation of the intestinal flora may be a promising new therapeutic option for atherosclerosis.

Mesenchymal stem cells (MSCs) are pluripotent stem cells that possess the remarkable ability for self-renewal and multidirectional differentiation. Their primary functions encompass differentiation, suppression of inflammation, and regulation of immune responses. Earlier studies have demonstrated that MSCs can raise the number and function of regulatory T cells (Treg cells), which have been shown to confer protective effects against AS [16,17]. Additionally, they can exert anti-AS effects by secreting anti-inflammatory factors and down-regulating the expression of costimulatory receptors on effector T cells, antigen-presenting cells, and NK cells [18,19]. Furthermore, MSCs are activated under hyperlipidemic conditions and differentiate into smooth muscle cells and adipocytes, which play a therapeutic role in cardiovascular diseases such as AS [20]. Mahdavi et al. postulated that MSCs exert a therapeutic effect against AS by modulating the degree of inflammation in the lesion [21]. Likewise, researchers have established that MSCs can play a reparative role in the heart by promoting M2 macrophage polarization and regulating the ratio of M1/M2 phenotype [22]. On the other hand, transplantation of MSCs resulted in increased secretion of anti-inflammatory factors (IL-10) and decreased secretion of pro-inflammatory factors (IL-1β) [23]. Taken together, this insinuates that MSCs protect against AS by stimulating the secretion of anti-inflammatory factors and suppressing the expression of inflammatory pathways. However, it is still unclear whether human umbilical cord mesenchymal stem cells can affect the stability of atherosclerotic plaque through the intestinal flora - inflammation pathway.

Therefore, hUC-MSCs were used in this study to treat atherosclerosis mouse models. The purpose is to explore the possible mechanism of hUC-MSCs to improve the stability of atherosclerotic plaque by regulating the intestinal flora by detecting the difference in species and abundance of intestinal flora between the treated and non treated mice, the difference in Young's modulus of atherosclerotic plaque fiber cap/arterial intima, and the expression level of NLRP3, IL-1β, and IL-18 in atherosclerotic plaque.

2. Method

2.1. Animal models and samples

33 ApoE$^{-/-}$ and 10C57BL/6J male mice were procured from Spelford (Beijing) Biotechnology Co., Ltd (SCXK Jing: 2019-0010) to serve as animal models and samples. To establish the atherosclerosis model, ApoE$^{-/-}$ mice were randomly divided into divide the mice into normal diet (ND), high-fat diet (HFD), and hUC-MSCs treatment (HFDM) groups, and C57BL/6J mice into a blank control group (BC). Both ND and BC groups were fed with normal diets, and HFD and HFDM groups were fed with high-fat diets (67.1 % breeding rodent feed, 14 % lard, 1 % cholesterol, 0.2 % bile salts, 8 % sucrose, 8 % yolk powder, 1.8 % pre-mixed feed, and 0.2 % propylthiouracil).When fed until 16 weeks, saline was injected into the tail vein of BC, ND and HFD groups, and 5×10^5 hUC-MSCs were injected into the tail vein of the HFDM group twice at a week interval. All mice were fed until 20 weeks, and were anesthetized and executed for sampling. Two frozen 20 μm-thick aortic sections were stored in a −80 °C freezer for biomechanical property testing of

plaque fibrous caps, and 5 μm-thick adjacent tissues were collected for pathological analysis [24]. hUC-MSCs were obtained from the Experimental Center for Tissue Engineering and Stem Cells, Guizhou Medical University, China.

2.2. Histopathological analysis

The 5 μm-thick tissue sections were acquired and subsequently dehydrated with anhydrous ethanol. The morphological features of the atherosclerotic plaques in the aortic root were then examined using a combination of hematoxylin-eosin staining (HE), oil red O staining, and Masson trichrome staining. This comprehensive analysis included an assessment of the degree of luminal stenosis, size of the lipid core, thickness of the fibrous cap and intima, plaque area, and collagen fiber content within the plaque. In addition, the expression level of inflammatory factors, namely NLRP3, IL-1β, and IL-18, was detected by immunohistochemistry and immunofluorescence. All primary antibodies were rabbit polyclonal antibodies (Affinity Biosciences, USA) at a concentration of 1 mg/ml, which were diluted at a ratio of 1:100 when used and incubated at 4 °C overnight.

2.3. Testing the Young's modulus of plaque fibrous caps using atomic force microscopy

To accurately determine the Young's modulus of plaque fibrous caps, a 20 μm thick section of the aortic root was obtained and visualized under an atomic force microscope (Nanowizard IV XP, Germany) in contact mode. The section was then mounted on an inverted fluorescence microscope to precisely locate the position of the plaque fibrous cap. Six 3 μm × 3 μm areas on the plaque fibrous cap were randomly selected for scanning, and the mean and standard deviation of the Young's modulus were calculated.

The test probe was AN-CSG10 (Appnano), which has a reflective surface coated with Au and a tapered tip. With a nominal spring constant of 0.11 N/M, the probe was able to accurately measure the Young's modulus of the plaque fibrous cap. The experiment was performed in PBS buffer throughout, with the slide fixed in a Petri dish.

2.4. Mechanical data analysis

The Hertz model is the standard model used for the analysis of AFM. The plotted force-displacement curves were analyzed using the Hertzian model to characterize the Young's modulus in different regions. The formulae are as follows:

$$F = \frac{E}{1-\nu^2}\frac{2\tan\alpha}{\pi}\delta^2$$

$$a = \frac{2\tan\alpha}{\pi}\delta$$

Where F represents the loading force, δ denotes the indentation depth, E is the modulus of elasticity, and v is the relaxation ratio, which is generally assumed to be 0.5 owing to the incompressibility of biological tissues. α represents half of the probe tip opening angle, which was set to 15° in this study. The tissue was considered to be homogeneous within each probed area [25]. This was used to characterize the Young's modulus at different locations.

2.5. Stool collection, DNA extraction, 16S rRNA sequencing, and quality control

The perianal area of the mice was sterilized with 75 % alcohol, and then the fecal samples were collected into sterile EP tubes and stored in a −80 °C refrigerator. The whole genomic DNA of the samples was extracted by the CTAB method [26] and diluted with sterile water. Then, the diluted genomic DNA was used as a template to amplify the 16s rRNA V3-V4 region. Subsequently, PCR amplification was performed using specific primers with barcodes, New England Biolabs' Phusion® High-Fidelity PCR Master Mix with GC buffer, and high-efficiency, high-fidelity enzymes to improve amplification efficiency and accuracy. Libraries were constructed using the TruSeq® DNA PCR-Free Sample Preparation Kit and quantified by Qubit and Q-PCR. Following this, they were sequenced using NovaSeq6000. Paired-end reads were assigned to samples based on their unique barcode and truncated by cutting off the barcode and primer sequence. They were subsequently merged using FLASH (V1.2.7, http://ccb.jhu.edu/software/FLASH/) [27] to obtain raw tags. The raw tags were quality filtered under specific filtering conditions to obtain high-quality clean tags according to the QIIME (V1.9.1, http://qiime.org/scripts/split_libraries_fastq.

html) [28] quality-controlled process. Afterward, chimeric sequences were detected and removed using vsearch (https://github.com/torognes/vsearch/) [29] against a reference database (Silva database, https://www.arb-silva.de/) [30] to retrieve effective tags.

2.6. Analysis of sequencing data

The Uparse software (Uparse v7.0.1001, http://drive5.com/uparse/) [31] was used for our sequence analysis. Sequences with ≥97 % similarity were assigned to the same OTUs. Representative sequences for each OTUs were screened for further annotation, and for each representative sequence, taxonomic information was annotated based on the Mothur algorithm using the SILVA database (http://www.arb-silva.de/) [32]. To investigate the phylogenetic relationship between different OTUs and differences in dominant species in different samples (groups), MUSCLE software (version 3.8.31, http://www.drive5.com/muscle/) [33] was used to perform multiple sequence comparisons. OTUs abundance information was normalized using a standard sequence number corresponding to the sample with the fewest sequences, based on which subsequent analyses of alpha diversity and beta diversity were performed. Alpha diversity

was applied to analyze the complexity of species diversity using QIIME (Version 1.7.0) and displayed with R software (Version 2.15.3). Unweighted Pair-group Method with Arithmetic Mean (UPGMA) Clustering was conducted using the QIIME software (Version 1.9.1). Non-Metric Multi-Dimensional Scaling (NMDS) was plotted and analyzed using the vegan package of R software (Version 2.15.3), along with canonical correlation analysis (CCA) and redundancy analysis (RDA). Based on the species abundance, correlation coefficient values (Pearson correlation coefficient, PCC) were calculated among the genera to obtain the correlation coefficient matrix, and the network diagram was depicted using graphviz-2.38.0. Functional annotation information was obtained using Tax4Fun software, which uses minimal 16S rRNA sequence similarity to the SILVA database sequences as the reference sequence.

2.7. Statistical analysis

All data were statistically analyzed using SPSS26.0 statistical software, and the SW test was used to test the normality of continuous variables. Variables following a normal distribution were presented as mean ± standard deviation, and the ANOVA was used to compare differences between groups, Least Significant Difference (LSD) method and Tamhane's T2 for post-test. Spearman correlation analysis was used for correlation test. Variables not following a normal distribution were expressed as median (upper and lower quartiles), and the non-parametric rank sum test (Wilcoxon and Mann-Whitney *U* test) was used to compare differences within and between groups. Categorical variables were expressed as frequency and rate (or composition ratio), and the chi-square test or Fisher's exact probability method was used to compare differences between groups. Morphological indicators were analyzed with Image J software.

3. Results

The atherosclerotic plaque mouse models deficient in ApoE$^{-/-}$ were established, and 16S rRNA gene sequencing technology was applied to analyze the community structure and abundance of intestinal fecal flora. Additionally, atomic force microscopy was employed to investigate the microscopic morphology and biomechanical properties of the fibrous cap in the mouse atherosclerotic plaque.

3.1. High-fat diet reduced atherosclerotic plaque stability and was reversed by hUC-MSCs

Hematoxylin-eosin staining was used to quantify the thickness of plaque intima-media and fibrous cap, oil red O staining to evaluate plaque area, and Masson trichrome staining to measure plaque collagen fiber content. Our findings revealed that mice on a high-fat diet exhibited a significantly thinner fibrous cap, a significantly thicker intima (Fig. 1A–D-E), a significantly larger plaque area

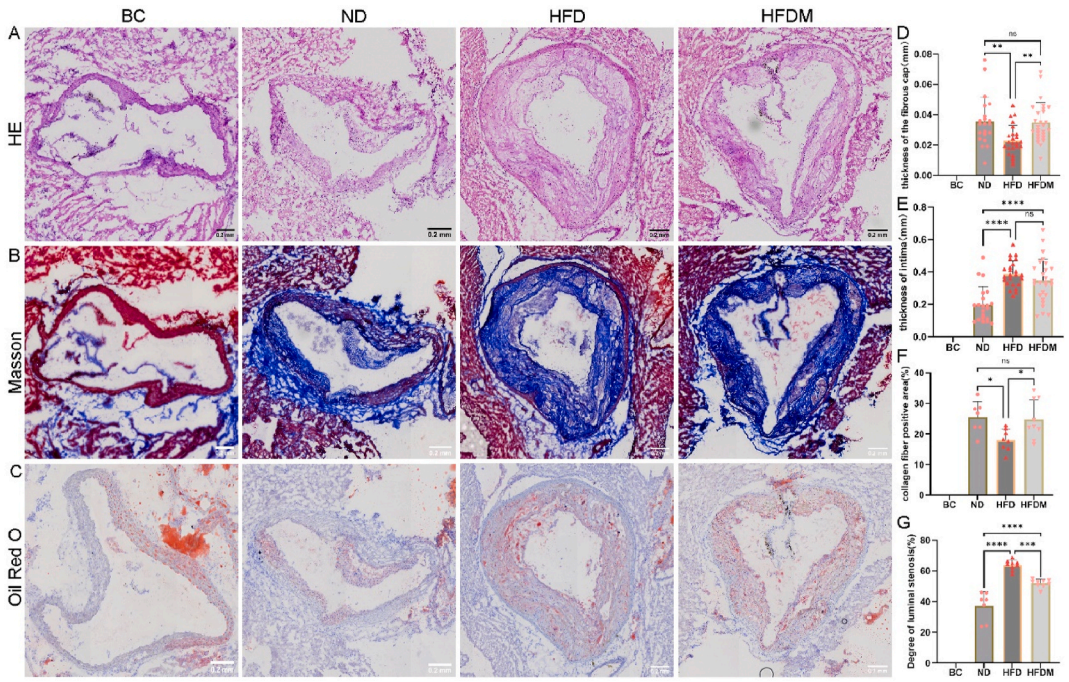

Fig. 1. Morphologic staining of the aortic root in mice (200 ×).Bar = 200 μm. **A**: hematoxylin-eosin staining (HE); **B**: oil red O staining; **C**: Masson staining. **D-E**: Quantification of Intima thickness and fibrous cap thickness by HE staining. **F**: Quantification of collagen fibers by Masson staining. **G**: Quantification of luminal stenosis by oil red O staining.*: P < 0.05, **: P < 0.01, ***: P < 0.001, ****:P < 0.0001. ns: no significance.

(Fig. 1C–G), and a significantly reduced collagen fiber content (Fig. 1B–F) compared to those in the control group. However, following hUC-MSCs intervention, the intimal thickness was decreased, and collagen fiber content and fibrous cap thickness were significantly increased, signaling that plaque stability was substantially enhanced (Fig. 1).

Immunohistochemistry and immunofluorescence assays were used to further explore the expression levels of the inflammatory factors NLRP3, IL-1β, and IL-18 in the atherosclerotic plaques of each group of mice. Immunohistochemical staining results demonstrated that the expression levels of NLRP3, IL-1β, and IL-18 were significantly higher in HFD compared with ND (Fig. 2A–C-E), consistent with the results of the immunofluorescence assay (Fig. 2B). Following hUC-MSCs intervention, the expression levels of NLRP3, IL-1β, and IL-18 were significantly down-regulated (Fig. 2).

Furthermore, the fibrous cap morphology map and Young's modulus of atherosclerotic plaques were examined in the four distinct groups using atomic force microscopy. Our findings revealed that compared to mice in the conventional diet groups (BC, ND), those in the high-fat diet group (HFD, HFDM) exhibited a fibrous cap tissue that was more intricately undulating, disorganized, and unevenly distributed, with a diminished Young's modulus and a decreased capacity to withstand the strain. This resulted in a relatively unstable plaque and a fibrous cap that was more prone to rupture (Fig. 3A). Additionally, correlation analysis was conducted between the Young's modulus of plaque fibrous cap and the Firmicutes/Bacteroidota(F/B) ratio of intestinal flora, which yielded a significantly negative correlation ($r = -0.70959$) (Fig. 3B).

3.2. *High-fat diet promoted structural changes in the intestinal flora and was reversed by hUC-MSCs*

After quality control and chimera removal, a total of 2053307 sequences were gathered, with an average of 73332 ± 4825.49 sequences per sample. On average, 71,601 sequences were successfully annotated to species, with an average of 1698 unique sequences per sample and an average of 647 OTUs (Fig. 4A). Species rarefaction curves were plotted by randomly extracting data from the sequencing data, which indicated that the sequencing depth and coverage were adequate and met the requirements for data analysis (Fig. 4B). To investigate species composition and abundance in each group of samples, a top 100 phylogenetic tree was constructed by comparing sequences, and the results indicated that the intestinal microorganisms were predominantly composed of Firmicutes, Bacteroidota, and Proteobacteria (Fig. 4D). At the phylum level, a cumulative bar plot of species abundance was generated based on the results of species annotation, which suggested a significant fluctuation in the structure of the intestinal flora in mice of the high-fat fed group (HFD, HFDM) compared to those of the control diet group (ND, BC) (Fig. 4C). More specifically, mice in the high-fat diet group (HFD, HFDM) had an increased proportion of Firmicutes, a decreased proportion of Bacteroidota, and consequently a significantly increased ratio of F/B compared to mice in the control diet group (ND, BC). Furthermore, a species clustering heat map was drawn based on species annotation and abundance information, depicting structural changes in the flora of mice at both the phylum and genus levels after a high-fat diet and again after MSC injection (Fig. 4E). At the genus level, the abundance of Lactobacillus

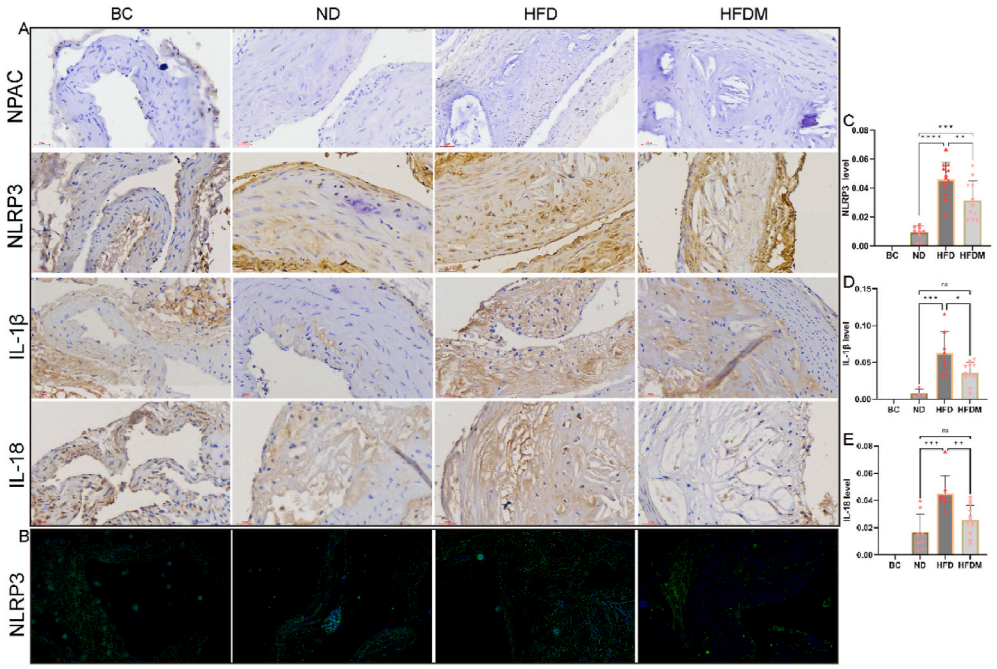

Fig. 2. Expression of inflammatory factors in aortic atherosclerotic plaques (400 ×). **A:** Immunohistochemistry of NLRP3, IL-1β, and IL-18 in atherosclerotic plaques. (NPAC: no primary antibody staining controls).Bar = 30 μm. **B:** Immunofluorescence of NLRP3 in atherosclerotic plaques. **C-E:** Quantification of NLRP3, IL-1β, and IL-18 by immunohistochemistry. *: $P < 0.05$, **: $P < 0.01$, ***: $P < 0.001$, ****:$P < 0.0001$. ns: no significance.

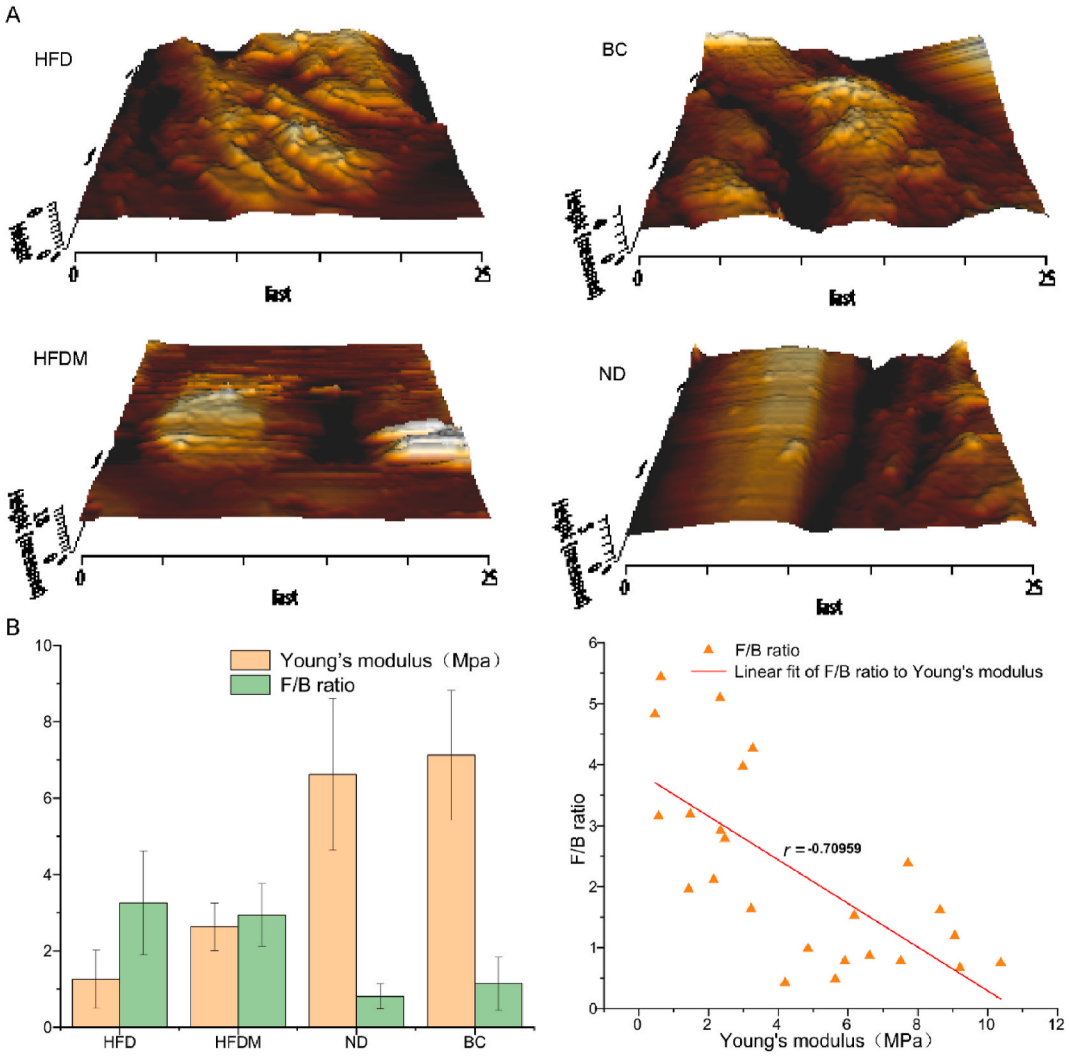

Fig. 3. AFM Testing of Atherosclerotic Plaque Fibrous Cap. **A:** The 3D morphology of the atherosclerotic plaque fibrous cap was analyzed in each group (25 × 25um). The height of the cap was measured, and the results were as follows: BC: 3.43 μm, ND: 3.73 μm, HFD: 8.37 μm, and HFDM: 7.28 μm. **B:** The Young's modulus of the atherosclerotic plaque fibrous cap and F/B ratio were analyzed for each group, and a linear fit was performed ($r = -0.70959$).

Dubosiella and Bacteroides, which play a decisive role in ameliorating atherosclerosis, was significantly increased in the HFDM group (Fig. 4D).

Furthermore, the intestinal flora species diversity was found to be significantly higher in the ND and BC groups compared to the HFD and HFDM groups, as indicated by OTUs, chao1, ACE, and other indices ($P < 0.05$). Although the ND group exhibited marginally greater indices than the BC group, the differences were not statistically significant ($P > 0.05$). However, the Shannon's index and Simpson's index were comparable between the groups (Table 1). To better illustrate the diversity discrepancies among the groups, a rank abundance curve was generated based on the relative abundance of OTUs. Interestingly, the plot mirrored the rarefaction curves, with the HFDM group exhibiting significantly higher species richness and distribution uniformity than the HFD group (Fig. 5A).

To establish inter- and intra-group distinctions in our sample, Non-Metric Multi-Dimensional Scaling (NMDS) analysis was carried out by utilizing the Bray-Curtis distance metric. The analysis exposed the aggregation of ND and BC, as well as HFD and HFDM (Fig. 5B). While group partitions were not overtly apparent in the NMDS downscaling analysis, the Anosim analysis based on Bray-Curtis distance values demonstrated that the differences between groups were significantly more pronounced than the intra-group differences within each group (Fig. 5C), signaling that our grouping methodology was practicable for this analysis.

To further investigate the relationship between the four groups, Unweighted Pair-group Method with Arithmetic Mean (UPGMA) clustering trees were developed based on weighted UniFrac distances. In agreement with the findings of prior studies, the HFDM group clustered with the HFD group, while the ND group clustered with the BC group. This implies significant alterations in intestinal flora between mice on a high-fat diet and those fed a normal diet. As depicted in Fig. 5D, the F/B ratio was significantly higher in the HFDM

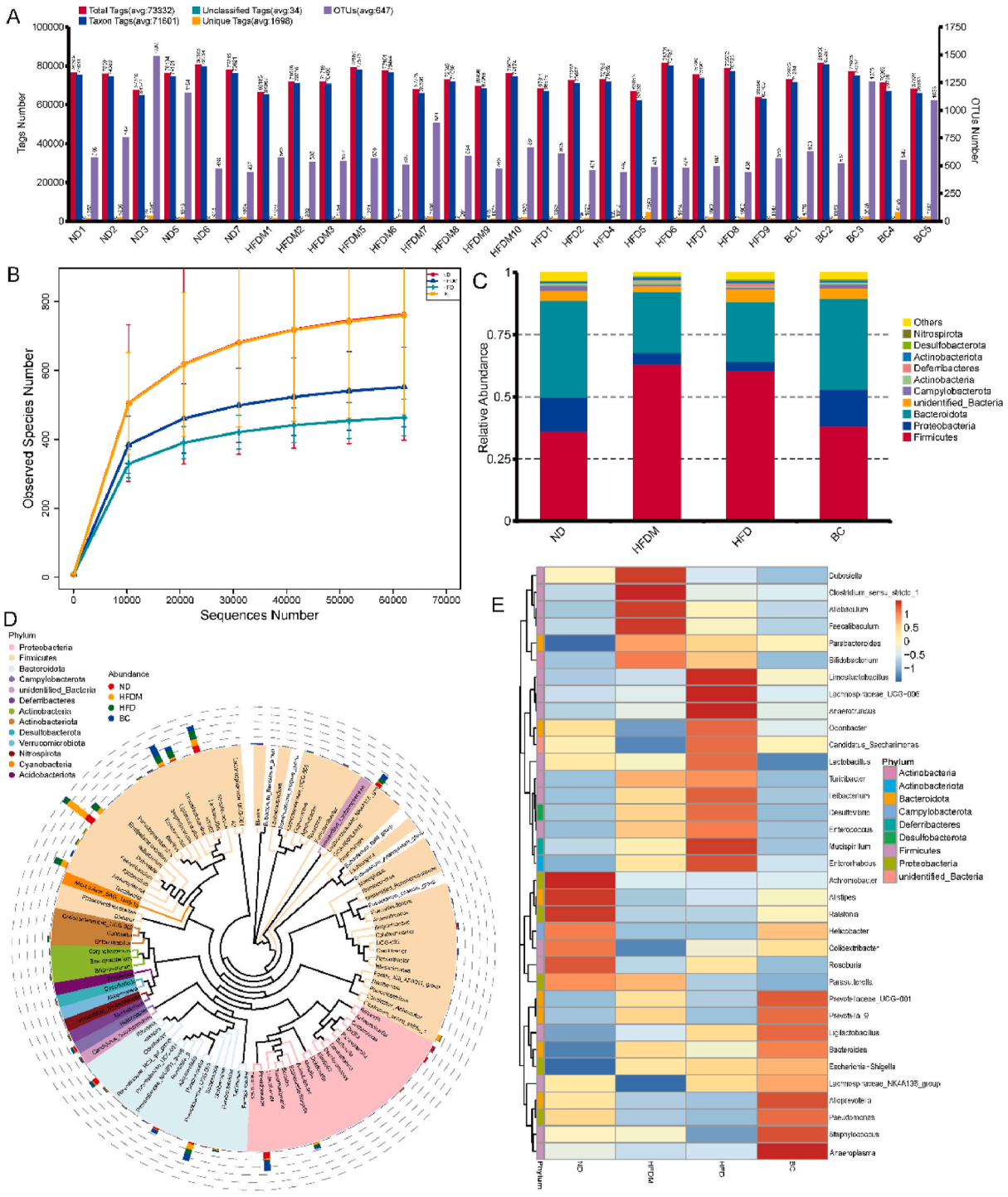

Fig. 4. High-fat diet and MSCs significantly altered intestinal flora composition. **A:** Statistical plot displaying individual sample sequences and OTUs after undergoing quality control. **B:** Rarefaction Curves for ND = 6, BC = 5, HFD = 8, HFDM = 9, randomly sampled sequences with newly discovered OTUs, with slopes close to zero in each group when sequencing depth was sufficient to cover the majority of the intestinal flora. **C:** Histogram showcasing the top 10 bacterial abundances for ND = 6, BC = 5, HFD = 8, and HFDM = 9. **D:** Phylogenetic tree of the top 100 bacterial genera in abundance at the genus level, with branch and sector colors representing their corresponding clades and stacked bars on the outside of the fan ring indicating information on the abundance distribution of the genus in different samples. **E:** The heat map of clusters drawn at the species level for the top 35 genera selected for abundance in all samples is displayed based on their abundance information in each sample. The clustering tree color denotes its corresponding phylum, and the color depth of the squares represents species abundance.

Table 1
Comparison of diversity indices of mice in each group.

group	OTUs	Shannon	Simpson	chao1	ACE	goods_coverage
BC	760[a]	5.874	0.927	805.059[b]	806.625[b]	0.999
HFD	463	5.46	0.923	482.48	486.995	0.999
HFDM	551	5.346	0.912	582.949[a]	583.188	0.999
ND	762[a]	6.084	0.94	809.928[a]	812.43[a]	0.999

OTUs: the number of species observed. **Shannon**: the total number of taxa in the sample and their proportion; the higher the diversity of the community, the more evenly distributed the species, the larger the Shannon index. **Simpson**: characterizes the diversity and evenness of species distribution within the community; the better the species evenness, the larger the Simpson index. **chao1**: estimates the total number of species contained in the community sample. **ACE**: estimates the number of OTUs in the community. **goods_coverage**: coverage; the higher the sequencing coverage, the larger the index.

[a] :$P < 0.05$ compared with the HFD group.

[b] :$P < 0.01$ compared with the HFD group.

and HFD groups compared to the ND and BC groups (Fig. 5D). To elucidate the effects of a high-fat diet and MSCs on the interactions between intestinal flora, Spearman correlation analysis of bacterial genera was performed at the genus level, and a flora correlation network was constructed using Cytoscape (Fig. 5E). The correlation network plot portrayed that the negative correlations between the groups of Firmicutes and Bacteroidota in mice on a high-fat diet were accentuated compared to the control group such as Dubosiella (F), Bacteroides (B), Lachnospiraceae_NK4A136_group (F), Alistipes (B), Ruminococcus_gauvreauii_group (F), Faecalibacterium (F). These observations inferred that high-fat diets disrupted the balance between the thick-walled phylum and the anaphyla phylum, leading to an imbalance in the normal ratio and causing phenotypic changes in the host. However, after intervention with hUC-MSCs, the negative correlations were reversed and even returned to normal levels.

To further identify distinctions among the intestinal microbiota of mice, MetaStat analysis was performed on the sequencing results of the four groups at the genus and species levels (Fig. 6A). Compared to the control diet group, the HFD groups exhibited a significant increase in the relative abundance of Ligilactobacillus, Mucispirillum, Limosilactobacillus, Anaerotruncus, Turicibacter, Escherichia-Shigella, Faecalibaculum, Bifidobacterium, Lactobacillus_murinus, Lactobacillus_reuteri, Escherichia_coli, Odoribacter, and 12 other species of bacteria. Conversely, the relative abundance of bacteria such as Alistipes, Alloprevotella, Staphylococcus, and Dubosiella was significantly decreased. Following treatment with hUC-MSCs, Lactobacillus_murinus, Lactobacillus_reuteri, Ligilactobacillus, Mucispirillum, Anaerotruncus, Lachnospiraceae_NK4A136_group, Odoribacter, Limosilactobacillus, Candidatus_Saccharimonas, and nine other bacterial species showed a significant decrease in relative abundance, whereas Alloprevotella, Clostridium_sensu_stricto_1, Staphylococcus, Faecalibaculum, Dubosiella, and other bacteria manifested a significant increase in relative abundance.

Finally, Tax4Fun was used to predict the function of the intestinal microbiota in the samples. In addition, a Venn Graph was plotted based on the results of gene function annotation, which demonstrated an increase in unique functional genes after hUC-MSCs treatment (Fig. 6B). What's more, the functional differences were insignificant between control groups (ND and BC groups) but were significant changes in cellular community - prokaryotes, genetic information processing, and infectious diseases in the HFD group compared to the control group. After treatment with hUC-MSCs, significant differences were identified in Replication and repair, Translation, Amino acid metabolism, Nucleotide metabolism, Energy metabolism, Metabolism of cofactors and vitamins, and Signal transduction (Fig. 6C). Collectively, these findings suggest that alterations in the function of intestinal microbiota due to a high-fat diet may contribute to the development of atherosclerosis.

4. Discussion

Currently, coronary heart disease (CHD) remains a pressing global issue. Atherosclerosis (AS) serves as the pathological basis of CHD, and the stability of the plaque formed by AS is a crucial factor in assessing the risk of sudden death from CHD. Following atherosclerosis, vessels typically compensate via vasodilation to maintain blood supply to downstream tissues [34]. Although downstream blood supply is not affected, the lumen gradually narrows as the atherosclerotic plaque increases in size, the vessel wall's ability to dilate is lost, and the lipid core is covered with proliferating vascular smooth muscle cells known as a fibrous cap. As the lipid core expands and the vessel wall's elasticity is lost, the thinner fibrous cap is more likely to rupture. Therefore, enhancing the plasticity of the fibrous cap may be a promising treatment strategy in patients with atherosclerosis. Recent studies primarily assessed plaque stability by measuring lipid core size and fibrous cap thickness [35]. However, the mechanical properties of the plaque fibrous cap are also key to assessing stability, and plaque rupture occurs when the mechanical stress to which the plaque is subjected is greater than its ultimate stress in a hemodynamic setting [36]. Therefore, there is an urgent need to accurately investigate the biomechanical properties of plaques and conduct a thorough and objective assessment of their stability to evaluate the likelihood of rupture. AFM is based on the measurement of very weak forces between the surface of the sample under test and the atoms on the probe with nanometer-level accuracy, allowing the acquisition of three-dimensional images at the microscopic level. It is extensively used in various fields, such as microbiology and ophthalmology [8,9].Therefore, AFM was used in the present study to measure the Young's modulus of the plaque fibrous cap in order to assess plaque stability and identify the differences in different groups of mice. In agreement with the observations of previous studies [11], our study found that the degree of atherosclerosis and plaque heterogeneity were significantly higher whereas the Young's modulus of the fibrous cap was significantly lower in mice of the high-fat diet group compared to those of the control diet group. Additionally, morphological examination of plaques uncovered significantly thinner fibrous caps, significantly

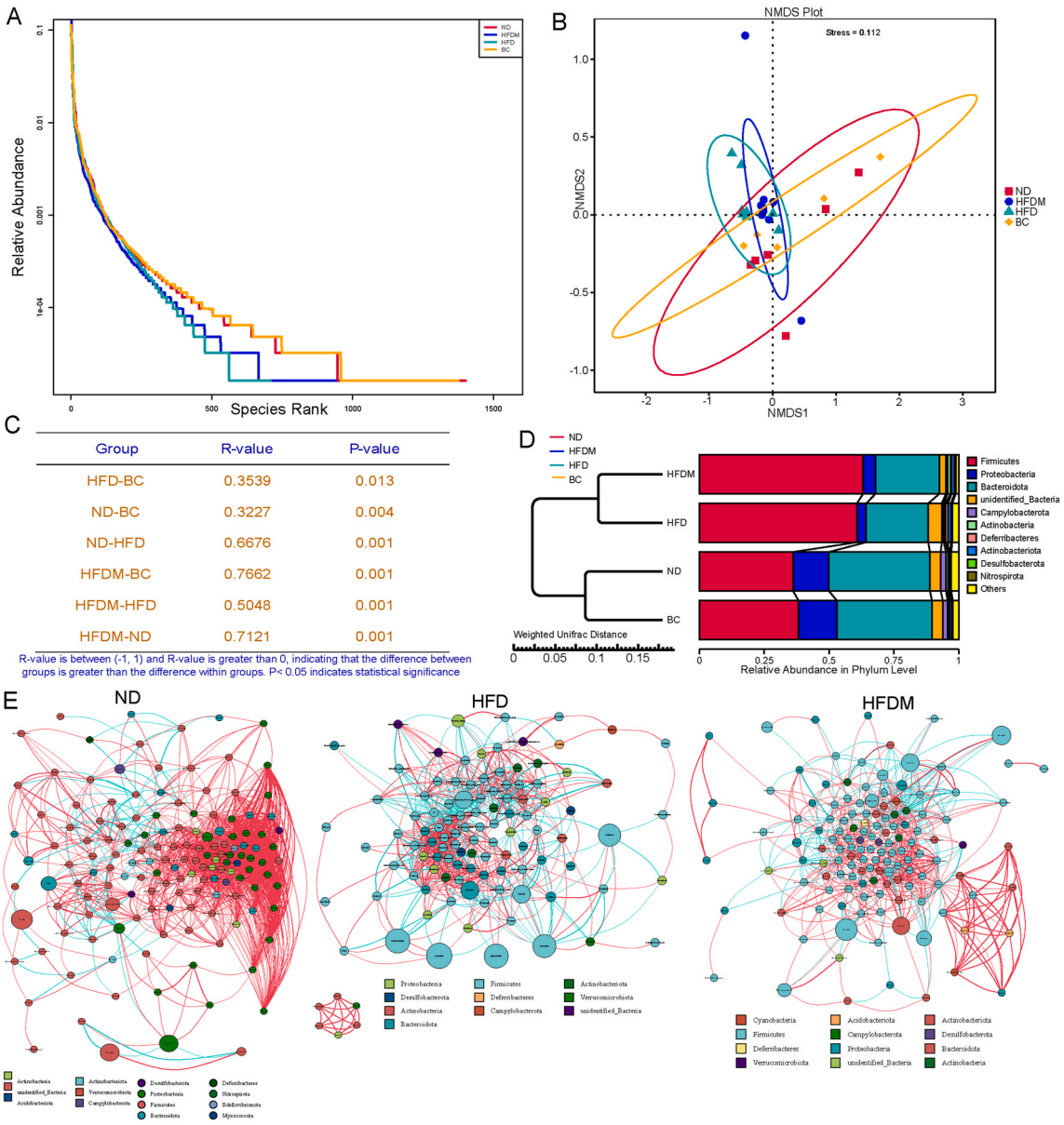

Fig. 5. Correlation between groups of mice intestinal flora. **A:** Rank Abundance curve based on the relative abundance of OTUs. A large slope of the curve and a shorter horizontal axis indicate poor species abundance and uniformity of distribution; on the contrary, a smaller slope and a longer horizontal axis indicate high species abundance and uniformity of distribution. **B:** Dimensionality reduction analysis based on Weighted UniFrac distance NMDS. Stress <0.2 suggests that NMDS can accurately reflect the degree of variation between samples. **C:** Anosim analysis based on Bray-Curtis distance values illustrated that the between-group differences of the groups were greater than the within-group differences. **D:** UPGMA clustering tree based on Bray-Curtis distance values. The UPGMA clustering tree structure is displayed on the left, and the relative abundance distribution of species at the phylum level for each sample is delineated on the right. **E:** Network diagram of the ND, HFD, and HFDM group clusters. Different nodes represent different genera, node size represents the average relative abundance of the genus, nodes of the same phylum have the same color, and the thickness of the line between nodes indicates correlation strength; red represents a positive correlation, whereas blue represents a negative correlation.

thicker intima, significantly larger plaque areas, and significantly lower collagen fiber content in mice of the high-fat diet group compared to those of the control diet group. In other words, the plaque area was significantly larger, and the collagen fiber content was significantly reduced. In this study, we did not count the proportion of ruptured plaques, and our conclusion was based on the proportion of vulnerable plaques.

It is universally acknowledged that microorganisms are present in various organs of the human body, particularly in the intestine. Currently, the relationship between intestinal flora and atherosclerosis is a hot topic, with numerous scholars endorsing the concept of

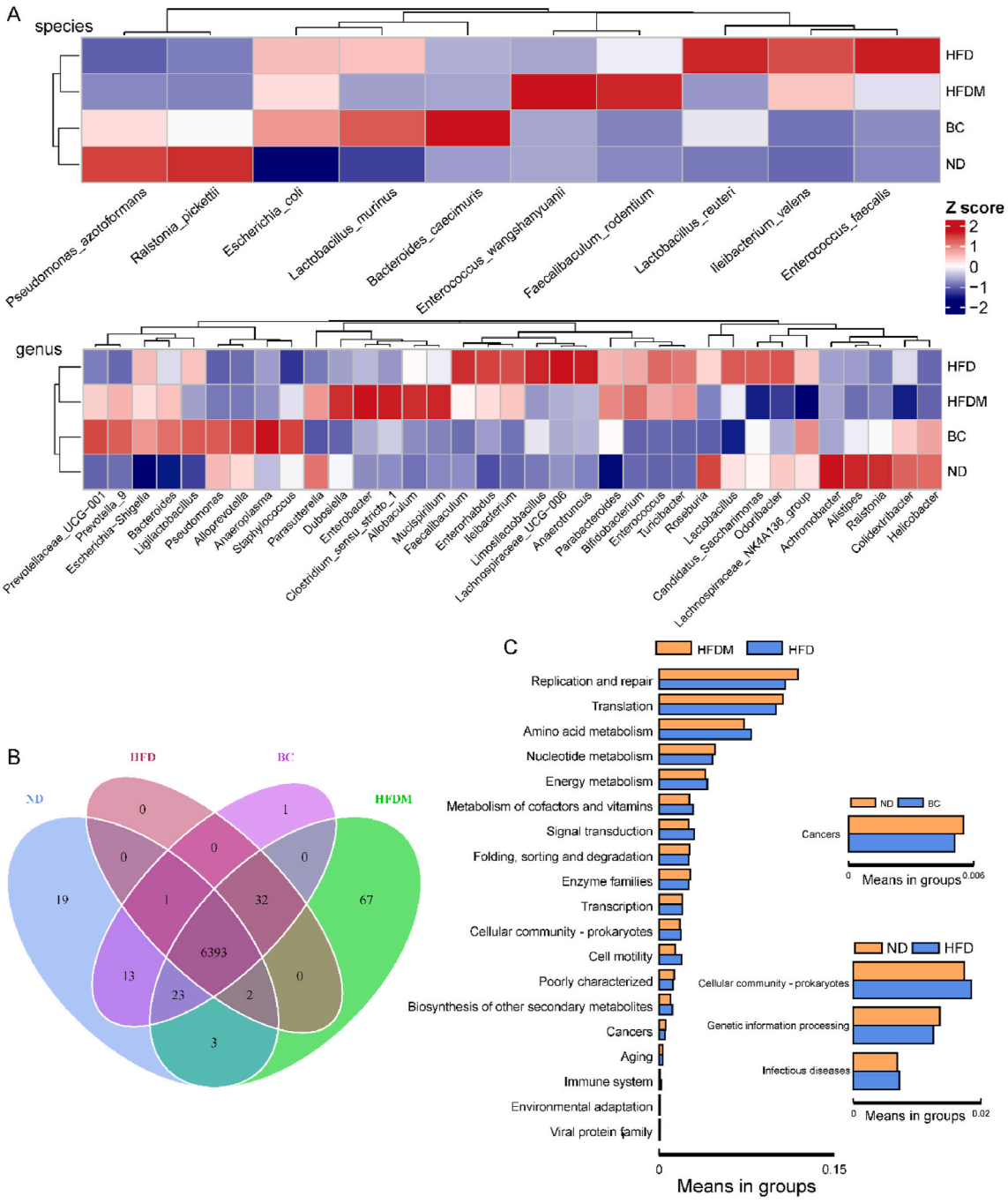

Fig. 6. Analysis of colony and functional differences. **A:** Heat map of colony differences at the genus and species levels. **B:** Venn Graph based on functional annotations to analyze the functional differences in flora between different groups. **C:** Tax4fun prediction of functional differences in intestinal flora genes in each group.

the gut-heart axis. Abnormal increases in intestinal flora metabolites, increased intestinal permeability, direct invasion and infection of lesions by intestinal microorganisms, and a consequential increase in butyrate- and short-chain fatty acid-producing bacteria have all been linked to the development and prevention of atherosclerosis [37,38]. Direct infection of the vascular wall, such as lipopolysaccharide (LPS), contributes to the onset of atherosclerosis. Indeed, LPS-treated mice develop more unstable plaques, and high levels of LPS in the blood are positively correlated with atherosclerosis [39,40]. The intestinal flora has a significant impact on the stability of atherosclerotic plaques by directly or indirectly mediating the host's intestinal structure, inflammatory status, and metabolic levels, thereby modulating the host's phenotype [41]. Firstly, alterations in the structural composition of the intestinal flora trigger

inflammation, which facilitates AS development [42]. Secondly, the regulation of host cholesterol levels and lipid metabolism by the gut flora affects the development of AS [43,44]. Thirdly, specific metabolites of the gut microbiota can exert beneficial or detrimental effects on AS (TMAO\LPS\SCFAs) [45]. Our study found that a high-fat diet led to dysbiosis in intestinal flora homeostasis, which was conducive to the development of atherosclerosis and plaque instability.

MSCs are presently being investigated in therapeutic studies for various diseases, including atherosclerosis. Previous studies have established that MSCs can alleviate atherosclerosis by modulating immune responses, differentiating into functional cells, and suppressing inflammation via multiple pathways [16,18,21]. Moreover, hUC-MSCs also have the advantages of low immunogenicity and immune escape [46], which gives it the ability to prevent the adverse reactions of the immune system, which is the advantage of hUC-MSCs over other types of stem cells [47]. Therefore, the possibility of hUC-MSCs injected into mice to cause a major immune response is low, so hUC-MSCs were used in our study. Our study concluded that MSC intervention resulted in structural adjustments in the composition of the intestinal flora of mice, reversing the abundance of some noxious flora induced by a high-fat diet. The ameliorative effect of hUC-MSCs on atherosclerosis does not exclusively rely on pathways modulating the immune response, functional cell differentiation, and inflammation but also by enhancing the biomechanical properties of the fibrous cap to counteract the mechanical blood flow.

Previous studies described a close relationship between the expression of inflammatory factors, the activation of inflammatory pathways, and atherosclerosis [48]. Therefore, the expression levels of NLRP3, IL-1β, and IL-18 were determined in the aortic atherosclerotic plaques of each group of mice. We found similar results with a significant increase in plaque NLRP3, IL-β, and IL-8 expression in mice on a high-fat diet, and a significant increase in plaque area, as well as a significant thinning of the fibrous cap, a decrease in collagen fibers, and a significant disruption of plaque. VSMC phenotypic transition owing to NLRP3 usually leads to changes in the mechanical properties of the fibrous cap. In our study, mice in the group with up-regulated NLRP3 levels had smaller Young's modulus of the fibrous cap, and the plaques were more susceptible to rupture by blood flow; that is, the plaques became unstable. The interaction between intestinal flora and NLRP3 also plays an instrumental role in atherosclerosis, suggesting a strategy to target NLRP3 and intestinal flora for the treatment of atherosclerosis [49]. Similarly, our study also validated the interrelationship between intestinal flora and NLRP3 inflammatory vesicles and further utilized hUC-MSCs targeting NLRP3 and intestinal flora to treat AS, with varying degrees of improvement in intestinal flora as well as plaque NLRP3 levels following treatment. In addition, a direct negative correlation was detected between the F/B ratio of the intestinal flora and the Young's modulus of the plaque fibrous cap, indicating that structural alterations in the composition of intestinal flora could lead to changes in the biomechanical properties of plaques, thereby affecting plaque stability. Treatment with hUC-MSCs delayed the changes in flora structure and mechanical properties of plaque brought about by a high-fat diet. In addition, the level of inflammation in the plaque correlated with its biomechanical properties and directly influenced the stability of the atherosclerotic plaque.

In summary, an AS model was established in ApoE$^{-/-}$ mice and 16s rRNA sequencing was subsequently used to detect structural changes in mouse microbiota. Our results exposed significant changes in the composition of the flora of mice in the HFD group, particularly an increase in Firmicutes abundance and a decrease in that of Bacteroidetes, leading to a significant increase in the F/B ratio, which is a commonly used index to assess homeostasis of the intestinal microbiota. The morphology of the fibrous cap and Young's modulus of atherosclerotic plaques in the four groups of mice were examined by atomic force microscopy, and the latter was found to be significantly lower in the HFD group. Alterations in intestinal flora homeostasis promoted the expression of NLRP3, which in turn affected VSMC phenotypic transition, leading to changes in their mechanical properties and ultimately a decrease in plaque stability. In contrast, hUC-MSCs intervention reversed the high-fat diet-induced imbalance in intestinal flora homeostasis, significantly down-regulated NLRP3 expression, significantly increased the Young's modulus of the fibrous cap, and thus contributed to plaque stability. This suggests that hUC-MSCs stabilized atherosclerotic plaques and effectively reduced the risk of atherosclerotic plaque rupture by regulating NLRP3 expression via modulating gut microbiota homeostasis.

There are two limitations in our research. Firstly, the wild-type C57BL/6J mice used in this study were not littermate controls, which may lead to the appearance of genetic drift. Secondly, the choice of our control group was not rigorous enough and normal chow fed ApoE−/− mice + hUC-MSCs should have been used as the control group instead of just normal chow fed ApoE−/− mice.

5. Conclusion

A high-fat diet led to dysregulation of intestinal flora homeostasis and induced abnormal expression of NLRP3, resulting in a decrease in plaque elastic modulus. However, hUC-MSCs improved the biomechanical properties of plaque by modulating the intestinal flora and NLRP3 expression, thereby increasing plaque stability and reducing the risk of plaque rupture. Conjointly, our study emphasizes the importance of a healthy diet and pioneered a novel approach for the treatment of AS.

Ethics statement

All animal experiments were supported by the Ethics Committee of Guizhou Medical University (No: 2,304,548).

Availability of data and materials

The datasets used and analyzed during the current study are available from the corresponding author on reasonable request.

Funding

This study was supported by National Natural Science Foundation of China (82,060,340); Guizhou Provincial Science and Technology Program (Qiankehe Foundation-ZK [2023] General 330); Guizhou Provincial General Higher Education Institutions Young Science and Technology Talent Growth Project (Qiankehe KY word [2021] 157); National College Student Innovation and Entrepreneurship Training Program (202,210,660,025); Key Laboratory of Evidence Forensics in Shandong Province Open subject (2018KFKT6).

CRediT authorship contribution statement

Lin Yang: Writing – original draft, Software, Formal analysis, Data curation. **Bing Xia:** Visualization, Investigation, Conceptualization. **Tianbao Qian:** Software, Resources, Data curation. **Jie Wang:** Supervision. **Yuanhe Wang:** Supervision. **Jialin Dai:** Supervision. **Cuiyun Le:** Visualization. **Xiaorong Yang:** Visualization. **Jun Wu:** Methodology. **Wenxin Wu:** Data curation. **Jianwei Xu:** Supervision, Resources. **Youbin Liu:** Supervision, Methodology. **Jiawen Wang:** Writing – review & editing, Supervision, Project administration, Funding acquisition.

Declaration of competing interest

The authors declare that they have no known competing financial interests or personal relationships that could have appeared to influence the work reported in this paper.

References

[1] G.A. Roth, G.A. Mensah, C.O. Johnson, G. Addolorato, E. Ammirati, L.M. Baddour, N.C. Barengo, A.Z. Beaton, E.J. Benjamin, C.P. Benziger, A. Bonny, M. Brauer, M. Brodmann, T.J. Cahill, J. Carapetis, A.L. Catapano, S.S. Chugh, L.T. Cooper, J. Coresh, M. Criqui, N. DeCleene, K.A. Eagle, S. Emmons-Bell, V.L. Feigin, J. Fernández-Solà, G. Fowkes, E. Gakidou, S.M. Grundy, F.J. He, G. Howard, F. Hu, L. Inker, G. Karthikeyan, N. Kassebaum, W. Koroshetz, C. Lavie, D. Lloyd-Jones, H.S. Lu, A. Mirijello, A.M. Temesgen, A. Mokdad, A.E. Moran, P. Muntner, J. Narula, B. Neal, M. Ntsekhe, G. Moraes de Oliveira, C. Otto, M. Owolabi, M. Pratt, S. Rajagopalan, M. Reitsma, A.L.P. Ribeiro, N. Rigotti, A. Rodgers, C. Sable, S. Shakil, K. Sliwa-Hahnle, B. Stark, J. Sundström, P. Timpel, I.M. Tleyjeh, M. Valgimigli, T. Vos, P.K. Whelton, M. Yacoub, L. Zuhlke, C. Murray, V. Fuster, Global burden of cardiovascular diseases and risk factors, 1990-2019: update from the GBD 2019 study, J. Am. Coll. Cardiol. 76 (25) (2020) 2982–3021.
[2] M. Pan, F. Zhang, K. Qu, C. Liu, J. Zhang, TXNIP: a double-edged sword in disease and therapeutic outlook, Oxid. Med. Cell. Longev. 2022 (2022) 7805115.
[3] J. Shin, J.E. Edelberg, M.K. Hong, Vulnerable atherosclerotic plaque: clinical implications, Curr. Vasc. Pharmacol. 1 (2) (2003) 183–204.
[4] K. Yahagi, F.D. Kolodgie, F. Otsuka, A.V. Finn, H.R. Davis, M. Joner, R. Virmani, Pathophysiology of native coronary, vein graft, and in-stent atherosclerosis, Nat. Rev. Cardiol. 13 (2) (2016) 79–98.
[5] N.V. Salunke, L.D. Topoleski, Biomechanics of atherosclerotic plaque, Crit. Rev. Biomed. Eng. 25 (3) (1997) 243–285.
[6] J. Ohayon, G. Finet, S. Le Floc'h, G. Cloutier, A.M. Gharib, J. Heroux, R.I. Pettigrew, Biomechanics of atherosclerotic coronary plaque: site, stability and in vivo elasticity modeling, Ann. Biomed. Eng. 42 (2) (2014) 269–279.
[7] S. Zhang, Y. Liu, Y. Cao, S. Zhang, J. Sun, Y. Wang, S. Song, H. Zhang, Targeting the microenvironment of vulnerable atherosclerotic plaques: an emerging diagnosis and therapy strategy for atherosclerosis, Adv Mater 34 (29) (2022) e2110660.
[8] S. Liu, Y. Wang, Application of AFM in microbiology: a review, Scanning 32 (2) (2010) 61–73.
[9] M. Milka, I. Mróz, M. Jastrzebska, R. Wrzalik, D. Dobrowolski, A.M. Roszkowska, L. Moćko, E. Wylegała, [Application of atomic force microscopy (AFM) in ophthalmology], Klin. Oczna. 114 (1) (2012) 71–74.
[10] Y. He, C. Qin, Z. Sun, Z. Liu, Y. Chen, K. Meng, Atomic force microscopy application to study of the biomechanical properties of the aortic intima in the context of early atherosclerosis, Microsc. Res. Tech. 85 (10) (2022) 3411–3417.
[11] A. Rezvani-Sharif, M. Tafazzoli-Shadpour, A. Avolio, Progressive changes of elastic moduli of arterial wall and atherosclerotic plaque components during plaque development in human coronary arteries, Med. Biol. Eng. Comput. 57 (3) (2019) 731–740.
[12] W.H.W. Tang, F. Bäckhed, U. Landmesser, S.L. Hazen, Intestinal microbiota in cardiovascular health and disease: JACC state-of-the-art review, J. Am. Coll. Cardiol. 73 (16) (2019) 2089–2105.
[13] P. Libby, D. Egan, S. Skarlatos, Roles of infectious agents in atherosclerosis and restenosis: an assessment of the evidence and need for future research, Circulation 96 (11) (1997) 4095–4103.
[14] N. Yoshida, T. Emoto, T. Yamashita, H. Watanabe, T. Hayashi, T. Tabata, N. Hoshi, N. Hatano, G. Ozawa, N. Sasaki, T. Mizoguchi, H.Z. Amin, Y. Hirota, W. Ogawa, T. Yamada, K.I. Hirata, Bacteroides vulgatus and Bacteroides dorei reduce gut microbial lipopolysaccharide production and inhibit atherosclerosis, Circulation 138 (22) (2018) 2486–2498.
[15] H. Liu, X. Chen, X. Hu, H. Niu, R. Tian, H. Wang, H. Pang, L. Jiang, B. Qiu, X. Chen, Y. Zhang, Y. Ma, S. Tang, H. Li, S. Feng, S. Zhang, C. Zhang, Alterations in the gut microbiome and metabolism with coronary artery disease severity, Microbiome 7 (1) (2019) 68.
[16] S.M. Fang, D.Y. Du, Y.T. Li, X.L. Ge, P.T. Qin, Q.H. Zhang, Y. Liu, Allogeneic bone marrow mesenchymal stem cells transplantation for stabilizing and repairing of atherosclerotic ruptured plaque, Thromb. Res. 131 (6) (2013) e253–e257.
[17] H. Ait-Oufella, B.L. Salomon, S. Potteaux, A.K. Robertson, P. Gourdy, J. Zoll, R. Merval, B. Esposito, J.L. Cohen, S. Fisson, R.A. Flavell, G.K. Hansson, D. Klatzmann, A. Tedgui, Z. Mallat, Natural regulatory T cells control the development of atherosclerosis in mice, Nat Med 12 (2) (2006) 178–180.
[18] M. Sharma, M.P. Schlegel, M.S. Afonso, E.J. Brown, K. Rahman, A. Weinstock, B.E. Sansbury, E.M. Corr, C. van Solingen, G.J. Koelwyn, L.C. Shanley, L. Beckett, D. Peled, J.J. Lafaille, M. Spite, P. Loke, E.A. Fisher, K.J. Moore, Regulatory T cells license macrophage pro-resolving functions during atherosclerosis regression, Circ. Res. 127 (3) (2020) 335–353.
[19] C. Spitz, H. Winkels, C. Bürger, C. Weber, E. Lutgens, G.K. Hansson, N. Gerdes, Regulatory T cells in atherosclerosis: critical immune regulatory function and therapeutic potential, Cell. Mol. Life Sci. 73 (5) (2016) 901–922.
[20] T. Chen, Y. Wu, W. Gu, Q. Xu, Response of vascular mesenchymal stem/progenitor cells to hyperlipidemia, Cell. Mol. Life Sci. 75 (22) (2018) 4079–4091.
[21] Gorabi A. Mahdavi, M. Banach, Ż. Reiner, M. Pirro, S. Hajighasemi, T.P. Johnston, A. Sahebkar, The role of mesenchymal stem cells in atherosclerosis: prospects for therapy via the modulation of inflammatory milieu, J. Clin. Med. 8 (9) (2019).
[22] D.I. Cho, M.R. Kim, H.Y. Jeong, H.C. Jeong, M.H. Jeong, S.H. Yoon, Y.S. Kim, Y. Ahn, Mesenchymal stem cells reciprocally regulate the M1/M2 balance in mouse bone marrow-derived macrophages, Exp. Mol. Med. 46 (1) (2014) e70.
[23] Z.X. Wang, C.Q. Wang, X.Y. Li, G.K. Feng, H.L. Zhu, Y. Ding, X.J. Jiang, Mesenchymal stem cells alleviate atherosclerosis by elevating number and function of CD4(+)CD25 (+)FOXP3 (+) regulatory T-cells and inhibiting macrophage foam cell formation, Mol. Cell. Biochem. 400 (1–2) (2015) 163–172.

[24] P. Tracqui, A. Broisat, J. Toczek, N. Mesnier, J. Ohayon, L. Riou, Mapping elasticity moduli of atherosclerotic plaque in situ via atomic force microscopy, J. Struct. Biol. 174 (1) (2011) 115–123.
[25] H.N. Hayenga, A. Trache, J. Trzeciakowski, J.D. Humphrey, Regional atherosclerotic plaque properties in ApoE-/- mice quantified by atomic force, immunofluorescence, and light microscopy, J. Vasc. Res. 48 (6) (2011) 495–504.
[26] X. Huang, N. Duan, H. Xu, T.N. Xie, Y.R. Xue, C.H. Liu, [CTAB-PEG DNA extraction from fungi with high contents of polysaccharides], Mol Biol (Mosk) 52 (4) (2018) 718–726.
[27] T. Magoč, S.L. Salzberg, FLASH: fast length adjustment of short reads to improve genome assemblies, Bioinformatics 27 (21) (2011) 2957–2963.
[28] N.A. Bokulich, S. Subramanian, J.J. Faith, D. Gevers, J.I. Gordon, R. Knight, D.A. Mills, J.G. Caporaso, Quality-filtering vastly improves diversity estimates from Illumina amplicon sequencing, Nat. Methods 10 (1) (2013) 57–59.
[29] T. Rognes, T. Flouri, B. Nichols, C. Quince, F. Mahé, VSEARCH: a versatile open source tool for metagenomics, PeerJ 4 (2016) e2584.
[30] B.J. Haas, D. Gevers, A.M. Earl, M. Feldgarden, D.V. Ward, G. Giannoukos, D. Ciulla, D. Tabbaa, S.K. Highlander, E. Sodergren, B. Methé, T.Z. DeSantis, J. F. Petrosino, R. Knight, B.W. Birren, Chimeric 16S rRNA sequence formation and detection in Sanger and 454-pyrosequenced PCR amplicons, Genome Res. 21 (3) (2011) 494–504.
[31] R.C. Edgar, UPARSE: highly accurate OTU sequences from microbial amplicon reads, Nat. Methods 10 (10) (2013) 996–998.
[32] Q. Wang, G.M. Garrity, J.M. Tiedje, J.R. Cole, Naive Bayesian classifier for rapid assignment of rRNA sequences into the new bacterial taxonomy, Appl. Environ. Microbiol. 73 (16) (2007) 5261–5267.
[33] R.C. Edgar, MUSCLE: multiple sequence alignment with high accuracy and high throughput, Nucleic Acids Res. 32 (5) (2004) 1792–1797.
[34] Y.S. Chatzizisis, A.U. Coskun, M. Jonas, E.R. Edelman, C.L. Feldman, P.H. Stone, Role of endothelial shear stress in the natural history of coronary atherosclerosis and vascular remodeling: molecular, cellular, and vascular behavior, J. Am. Coll. Cardiol. 49 (25) (2007) 2379–2393.
[35] K. Sakakura, M. Nakano, F. Otsuka, E. Ladich, F.D. Kolodgie, R. Virmani, Pathophysiology of atherosclerosis plaque progression, Heart Lung Circ. 22 (6) (2013) 399–411.
[36] R.A. Baldewsing, J.A. Schaar, F. Mastik, A.F.W. van der Steen, Local elasticity imaging of vulnerable atherosclerotic coronary plaques, Adv. Cardiol. 44 (2007) 35–61.
[37] H. Bartolomaeus, V. McParland, N. Wilck, [Gut-heart axis : how gut bacteria influence cardiovascular diseases], Herz 45 (2) (2020) 134–141.
[38] W. Chen, S. Zhang, J. Wu, T. Ye, S. Wang, P. Wang, D. Xing, Butyrate-producing bacteria and the gut-heart axis in atherosclerosis, Clin. Chim. Acta 507 (2020) 236–241.
[39] Z. Pan, Z. Fan, J. Ma, H. Liu, L. Shen, B. He, M. Zhang, Profiling and functional characterization of circulation LncRNAs that are associated with coronary atherosclerotic plaque stability, Am J Transl Res 11 (6) (2019) 3801–3815.
[40] J.E. Jaw, M. Tsuruta, Y. Oh, J. Schipilow, Y. Hirano, D.A. Ngan, K. Suda, Y. Li, J.Y. Oh, K. Moritani, S. Tam, N. Ford, S. van Eeden, J.L. Wright, S.F. Man, D. D. Sin, Lung exposure to lipopolysaccharide causes atherosclerotic plaque destabilisation, Eur. Respir. J. 48 (1) (2016) 205–215.
[41] K. Kiouptsi, C. Reinhardt, Contribution of the commensal microbiota to atherosclerosis and arterial thrombosis, Br. J. Pharmacol. 175 (24) (2018) 4439–4449.
[42] Z. Al Bander, M.D. Nitert, A. Mousa, N. Naderpoor, The gut microbiota and inflammation: an overview, Int. J. Environ. Res. Publ. Health 17 (20) (2020).
[43] M. Vourakis, G. Mayer, G. Rousseau, The role of gut microbiota on cholesterol metabolism in atherosclerosis, Int. J. Mol. Sci. 22 (15) (2021).
[44] M. Schoeler, R. Caesar, Dietary lipids, gut microbiota and lipid metabolism, Rev. Endocr. Metab. Disord. 20 (4) (2019) 461–472.
[45] M. Witkowski, T.L. Weeks, S.L. Hazen, Gut microbiota and cardiovascular disease, Circ. Res. 127 (4) (2020) 553–570.
[46] W. Jiang, J. Xu, Immune modulation by mesenchymal stem cells, Cell Prolif. 53 (1) (2020) e12712.
[47] J. Gopalarethinam, A.P. Nair, M. Iyer, B. Vellingiri, M.D. Subramaniam, Advantages of mesenchymal stem cell over the other stem cells, Acta Histochem. 125 (4) (2023) 152041.
[48] Y. Zhu, X. Xian, Z. Wang, Y. Bi, Q. Chen, X. Han, D. Tang, R. Chen, Research progress on the relationship between atherosclerosis and inflammation, Biomolecules 8 (3) (2018).
[49] X.N. Zhang, Z.L. Yu, J.Y. Chen, X.Y. Li, Z.P. Wang, M. Wu, L.T. Liu, The crosstalk between NLRP3 inflammasome and gut microbiome in atherosclerosis, Pharmacol. Res. 181 (2022) 106289.